Eng. Sci., 2025, **35**, 1540

Engineered Science
DOI: https://dx.doi.org/10.30919/es1540

Application of Artificial Neural Network for the Prediction of Pool Boiling Heat Transfer Coefficient of Nanofluid with External Magnetic Field Effect

Jarinee Jongpluempiti,[1] Ponthep Vengsungnle,[2] Sahassawas Poojeera,[2] Nittaya Naphon,[3] Smith Eiamsa-ard[4] and Paisarn Naphon[5,*]

Abstract

Analyzing the pool boiling heat transfer of nanofluids with artificial neural network (ANN) is the primary goal of this research, which also intends to conduct experimental investigations. The trials were conducted with magnetic fields ranging from 0.0008 to 0.0012 Tesla and nanofluid concentrations from 0.015 to 0.075 vol%. The pressure inside the chamber might be anything from 50 to 150 kPa. Before conducting an ANN analysis, a training session was conducted to teach the network how to estimate the pooled boiling heat transfer performance of mixes containing nanoparticles of TiO2 and refrigerant R141b in the presence of a magnetic field. There is evidence that the strength is greatly impacted by particle Brownian motion, which results in improved heat transfer. The heat transfer coefficient is greatly affected by pressure. The structure of the ANN model consists of four input neurons, two hidden layers, and one output neuron. Seventy percent of the 468 datasets are used for training, while the remaining 15% and 15% are divided equally between testing and validation. Given that the root mean deviation was only ±5%, it was enough for sensitivity. This method reduces the network's training time while increasing calculation efficiency. This architecture performs when training neural networks for classification and forecasting tasks that need accuracy and efficiency in tuning.

Keywords: Artificial neural network analysis; Magnetic fields; Boiling heat transfer; Nanofluids.
Received: 05 April 2025; Revised: 03 May 2025; Accepted: 14 May 2025.
Article type: Research article.

1. Introduction

The problem of heat dissipation from electronic devices has assumed new importance due to the ever-increasing heat output from ever-smaller components. Because of their low heat transfer capability, these conventional fluids cannot implement various strategies to enhance heat transmission. To improve passive heat transfer, one can change the boundary conditions, change the flow shape, or increase the thermophysical properties of the working fluids. The suspension of nanoparticles alters the thermal and transport properties of the base fluid. Several articles have detailed the heat transfer properties of nanofluids in a magnetic field (MF). There has been a flurry of research on how MF affects pool boiling heat transfer fluid. For an experimental study, Lee *et al*.[1] studied the potential for improving critical heat flux (CHF) utilizing magnetic-water nanofluids in electrically generated MF. Since they found that magnetic field improved the CHF values, they concluded that magnetic-water nanofluids are more economically viable than other nanofluids because MF can raise the local concentration of these nanofluids. The consequences of applying MF to a cylinder filled to the brim with boiling ferrofluid were investigated by Khosh Mehr *et al*.[2] The results showed that ferrofluid had a lower critical heat flux than water. It was also discovered that repeating the experiments under identical conditions reduces the sample's quenching time. Implementing the magnetic field at a

[1]*Department of Agricultural Machinery Engineering, Faculty of Engineering and Architecture, Rajamangala University of Technology Isan, Nakhonratchasima, 30000, Thailand*
[2]*Department of Mechanical Engineering, Faculty of Engineering, Rajamangala University of Technology Isan, Khon Kaen Campus, 40000, Thailand*
[3]*Department of Pharmaceutical Chemistry, Faculty of Pharmacy, Srinakharinwirot University, 63 Rangsit-Nakhornnayok Rd., Ongkharak, Nakhorn-Nayok, 26120, Thailand*
[4]*Department of Mechanical Engineering, Faculty of Engineering, Mahanakorn University of Technology, Bangkok, 10530, Thailand*
[5]*Department of Mechanical Engineering, Faculty of Engineering, Srinakharinwirot University, 63 Rangsit-Nakhornnayok Rd., Ongkharak, Nakhorn-Nayok, 26120, Thailand*
* *E-mail:* paisarnn@g.swu.ac.th (P. Naphon)

predetermined and continuous intensity significantly increased film boiling heat flux.

Researchers examined the effects of ferrofluid concentration on boiling and MF application. The investigational 10-aspect ratio silver cylinder was heated to 350 °C before being quenched in the ferrofluid. A rectangular cubic magnet was positioned above the fluid container to apply a magnetic field. They observed particle movement in the base fluid and a significant increase in film boiling heat flow following the application of the field. According to their results, a growing magnetic field causes the Nusselt number to decrease. Considering the morphological changes on the heated surfaces, Shojaeian *et al*.[3] examined magnetic fluids that pooled with the magnetic field. According to their research, the two-phase heat transfer coefficient is larger in a magnetically activated system compared to a system without MF. This is because the former causes high thermal fluxes.

Boiling heat transfer properties of ferrofluid were experimentally examined by Abdollahi *et al*.[4] concerning the MF. According to their findings, a negative magnetic field gradient raises the boiling temperature, while a positive gradient decreases it. The boiling heat transfer coefficient of the nanofluids with a concentration of 0.1% rises by about 6% and 13%, respectively, due to the negative magnetic gradient. Ozdemir *et al*.[5] studied the boiling heat transfer behavior. Using MF to generate an upward force at low heat fluxes speeds up the bubble detachment process. MF is anticipated to impact the boiling process because the aforementioned parameters significantly affect the boiling behavior.[6-9] Researchers have also computed the effects of MF on pool boiling characteristics. A numerical investigation on the boiling heat transfer of ferrofluid on a heater plate was carried out by Mohammadpourfard *et al*.[10,11] They investigated how the MF directions affected the bubble form by utilizing additional equations for mass transfer and magnetic field effects. The working fluid properties, surface characteristics, and operating conditions affect the boiling point and flow rate. The numerical results are remarkably consistent with the experimental data. In the next phase, this approach was utilized to investigate nanofluids containing alumina nanoparticles.

When compared to experimental data, the resulting results outperform silica nanofluid. Shuchi *et al*.[12] focused on this topic in their experimental investigation of the high-temperature boiling fluid flow characteristics with MF generated by solenoidal electromagnets. According to their findings, applying MF to the heated region's inlet may boost the heat transfer rate by as much as 140 % and less than 40 % for the outlet zone. Sami *et al*.[13] performed on the flow boiling of some refrigerants in side-increased surface tubing with the effects of magnetohydrodynamics. They suggested correlations to predict how the magnetic field affects average heat transfer coefficients and flow resistance. Using magnetic nanofluids in conjunction with magnetic fields generated by permanent neodymium magnets, Lee *et al*.[14,15] explored the potential for improving the flow boiling characteristics. They found that depositing magnetite nanoparticles onto a heated surface increased the flow boiling wettability and re-wetting qualities. A study conducted by Aminfar *et al*.[16] studied the effect of quadrupole MF on the flow boiling of a ferrofluid. The results showed that applying a magnetic field increased CHF values in both pure water and ferrofluids. The main causes for this effect of the magnetic field are changes in water characteristics caused by the magnetic field, improved single-phase convection heat transfer, suppression of nucleate boiling, and stabilization of boiling flow. In their study, Amirzehni *et al*.[17] found that bubbles grew more subtly when the magnetic field was present during flow boiling. They also investigated how MF affected the bubble departure width in flow boiling. They found that applying a magnetic field reduced the bubble size by 5-10 % and that the impact of the magnetic field on the bubble size was more substantial at more significant mass fractions. A magnetic field raises the surface tension, which keeps bubbles around and makes the flow more consistent.

Aminifar *et al*.[18] examined the numerical behavior of subcooled flow boiling of R113-based ferrofluids. They looked at how different axial magnetic gradients, both positive and negative, affected the distribution of void percentage, temperature, velocity, and pressure. Applying a magnetic field with a negative gradient reduced the evaporation rate, which caused the wall to dry out; as a result, they anticipated higher critical heat flux values. Mirzaee *et al*.[19] analyzed the impact of electrohydrodynamic (EHD) on the formation of steam bubbles. While an opposing Lorentz force enhances bubble production, a positive force slows and delays it. Mohammadpourfard *et al*.[20] statistically studied the properties of the ferrofluids flow boiling in a vertical annulus with nonuniform transverse MF. The MF increases the frequency of bubble separation by drawing the fluid toward the outside wall. Wong *et al*.[21] performed an order-of-magnitude study to determine the significance of the bubble phenomena. The analytical results are utilized to determine the impact of strong magnetic fields on nucleate boiling heat transfer. Kamiyama *et al*.[22] investigated boiling flow properties with magnetic fields. In a nonuniform magnetic field, the properties of boiling two-phase flows can be seen using ultrasonic wave echo, and different distributions of these flows' traits can be extracted. The theoretical and experimental investigation of the effect of a nonuniform magnetic field on the stability of boiling two-phase pipe flow of a magnetic fluid is carried out. These ground-breaking investigations demonstrate that by efficiently utilizing the magnetic field of a magnetic fluid, it is feasible to control and stabilize boiling two-phase flows in such a fluid.

Machine learning is the study of statistical algorithms that can gather knowledge from existing data and apply it to new, unknown data. The goal of this subfield of AI is to create machines that can carry out actions in the absence of human guidance. In recent years, heat transfer research has been a proliferation, using artificial neural networks to evaluate

experimental data. In machine learning, deep learning techniques rely on neural networks. Countless heat transfer applications have found success with artificial neural networks. These include solar energy, design of steam plants, heat loads, predicting airflow, thermal process analysis, plate and double pipe heat exchangers, and control power system.[23] Using trained artificial neural networks (ANN) to simulate thermal processes is a fast and accurate way to forecast their performance. Modeling using artificial neural networks has many advantages, such as better performance with sparse and noisy input data and more accurate approximations of complicated issues. Through ANN, several thermal researchers have gained access to measured data.[24] Researchers analyzed several heat exchanger types using ANN.[25-27] ANN performance study has been conducted on cooling towers and coverage-diverge tubes.[28] This ANN model showed good statistical performance with a correlation coefficient ranging from 0.993-0.999 and very low mean square error (MSE) values for ANN training and predictions compared to the experimental range. The use of ANNs to predict thermal performance has been reported in a few publications.[29,30] Findings from this study corroborate previous findings from experiments showing that the ANN model can make accurate thermal conductivity predictions. In their study, Ghahdarijani *et al*.[31] used ANN to predict the thermal performance of heat exchangers. Comparing statistical criteria, the multilayer perception (MLP) network with one hidden layer and 10 neurons, trained with the Levenberg-Marquardt (LM) algorithm, is the most effective for forecasting the convective heat transfer coefficient. Using the LM training technique, the MLP network with two hidden layers and six neurons per layer predicted pressure drop values that matched experimental results. The investigations by Naphon *et al*.[32-35] studied nanofluid flow and thermal performance using artificial neural networks in various heat transfer devices. Results from the artificial neural network and the current experiment are compared. Among training algorithms, Levenberg-Marquardt Backpropagation has the lowest mean square error (MSE) and highest correlation coefficient (R). Most data comes within ±2.5% and ±5% of the Nusselt number and friction factor, according to the best ANN model. A magnetic field-based spirally coiled tube's thermal performance was predicted using the optimal ANN.

Using an ANN technique, Longon *et al*.[36] evaluated the efficiency of the heat exchanger using nanofluids as coolant. Including cluster average size in input variables enhances ANN nanofluid thermal conductivity model prediction, although this parameter is often absent from published data. The paper details the ANN model parameters. In their study, Ahmadi *et al*.[37] used ANN to analyze the pressure drop of nanofluids in an automobile radiator. Multiple tests and errors are needed to determine neural network model parameters. The parameters were optimized using a genetic algorithm. In neural network optimization, this method's radiator pressure drop was examined. Neural networks can accurately simulate and estimate nanofluid flow pressure drop in the examined system. Sadeghzadeh *et al*.[38] used ANNs to predict the solar collector performance using nanofluids as coolant. Although other produced models can also accurately forecast the solar collector's efficiency, the MLP-ANN model yields the best thermal performance prediction, according to the results of the constructed models. Panda *et al*.[39] illustrated how artificial neural networks function by optimizing the heat transfer rate, especially under particle concentration. This study investigates the potential for combining the effects of concentrations in water, considering a wide range of factors that influence flow dynamics. The heat transfer rate analysis reaches optimal performance concerning the Nusselt number by using ANN and including many parameters. Ali *et al*.[40] studied the Darcy-Forchheimer flow behavior of double-hybrid nanofluids on a Riga plate about radiation and heat sources. Through training, validation, and testing, we enhance physical data sets using ANN, ensuring reliable data and an inclusive research methodology. Alklaibi *et al*.[41] used the hybrid nanofluids as a coolant and tested plate heat exchangers for their experimental study. Yaseen *et al*.[42] studied the steady, incompressible, and axisymmetric bioconvective flow of an Ag TiO_2/water hybrid nanofluid between two infinitely spinning disks. Flows between two rotating disks are used in evaporators, gas turbines, atomizers, computer disks, motors, and rotating air cleaners. A Darcy-Forchheimer porous media was utilized to explore the effects of a magnetic field, heat source, and thermal radiation. A similarity transformation transforms The controlling mathematical equations into connected nonlinear ordinary differential equations (ODEs). These equations are numerically solved using MATLAB's tool. An ANN model using multilayer perceptrons predicts the Nusselt number (heat transfer rate) on the disk's upper and lower surfaces. The model trains the ANN using the proven Levenberg-Marquardt method. Ismail *et al*.[43] looked at heat transfer through a ternary hybrid nanofluid (THNF) between a cone and a rotated disk. The authors incorporated radiation, Hall effects, and magnetic fields into their mathematical model to simulate the flow of THNF in a space between a cone and a disk. With the help of an ANN, this research improves the accuracy and resilience of predicting Nusselt values at cone and disk surfaces.

As previously stated, several studies have demonstrated the use of ANN in studying diverse thermal systems. ANNs have multiple benefits, making them an effective tool in various domains, including machine learning, data analysis, and artificial intelligence. Here are several significant advantages: ANNs can model complex, nonlinear input-output interactions, making them helpful in many applications. ANNs can handle noisy and missing data, allowing them to perform well. ANNs may generalize from training to new data, making them useful in predictive modeling. Parallel processing in ANNs may speed up calculations and allow them to handle large datasets. ANNs can handle photos, text, and time series, making them valuable for many applications. ANNs may find data patterns

and structures without programming, simplifying modeling. Big data applications suit ANNs because they can handle larger datasets and more complex models. Programmable ANNs can learn from new data and adapt to changing conditions to improve. Some papers have already mentioned how ANN may be used to investigate various thermal systems. However, there has been no success in using ANN to predict nanofluids pool boiling heat transfer with or without the magnetic field effect. The present work aims to experimentally investigate the pool boiling performance of R141b/nanoparticles. The experiments were carried out with nanofluid concentrations ranging from 0 to 0.075 vol%, chamber pressures ranging from 50 to 150 kPa, and magnetic fields ranging from 0.0008 to 0.0012 Tesla. The experimental findings were compared to those of other working fluids,[44,45] and an ANN analysis was done.

2. Experimental apparatus and procedure

2.1 Experimental apparatus

Fig. 1 shows the major components of the experimental test loop. The primary test pool is a 300 mm Pyrex glass container with an 80 mm inside diameter and a 10 mm Bakelite lid. The boiling surface is a metal cylindrical heater with a diameter of 12.7 mm and a length of 42 mm. The boiling surface temperature is measured using six type-T thermocouples. With an accuracy of 0.01 °C, a dry-block temperature calibrator has already pre-calibrated all the thermocouple probes. By modifying the flow rate of the coolant, the pressure transducer can monitor the boiling pressure in the test pool to within 0.02% of full scale. A storage tank, a pump, and a mechanism to monitor the flow rate make up the closed-loop of coolant. The boiling fluid is a refrigerant nanofluid. The calibration technique directly compares all sensors to the primary thermometer in the block calibrator insert.

The permanent Neodymium magnet, with details shown in Table 1, is used as the magnetic source. Average magnetic strength is measured by using the Triaxial Magnetic Field Meter (TM-192). Before recording data, the experimental system can approach the steady state where the relevant parameters are measured five times. The system generates a magnetic field between 0.8 and 1.2 × 10^{-4} Tesla using permanent neodymium magnets. It can be seen that the alignment of the magnets in this research is shown in Fig. 1.[44,45] Digital ammeters and voltmeters measure the heat input. Both the ammeter and the voltmeter are accurate to within 0.1 volts. The process may start the testing as soon as the bulk temperature of the boiling fluid sets.

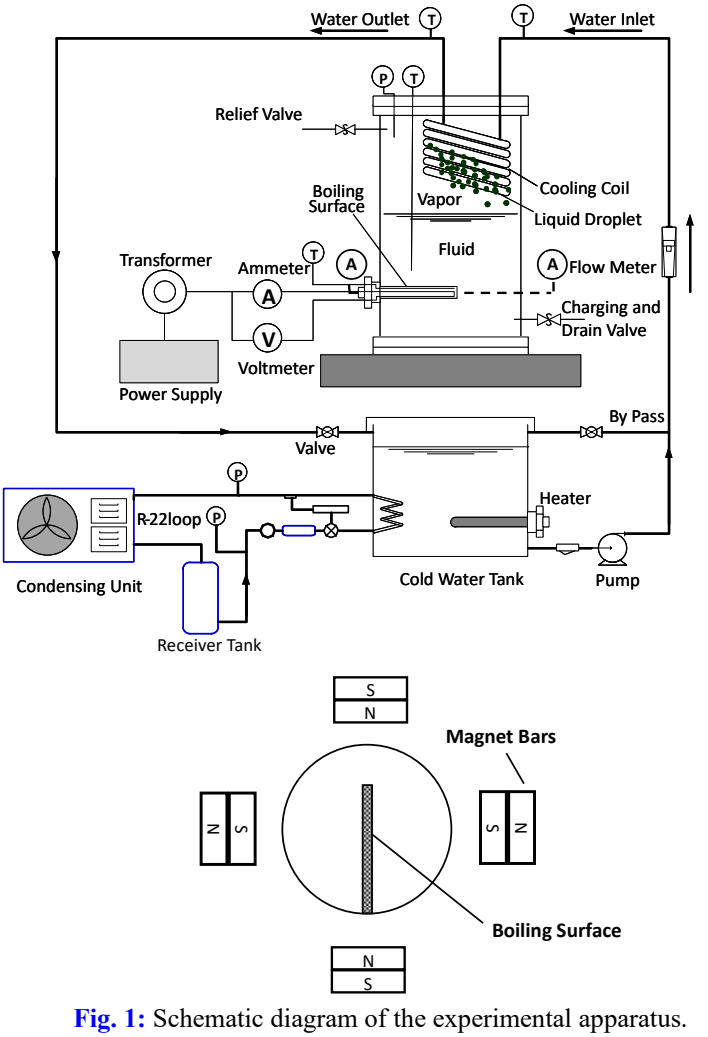

Fig. 1: Schematic diagram of the experimental apparatus.

Table 1: Details of permanent magnetic bars.

Parameters	Dimensions
Length (mm)	50
Width (mm)	50
Thickness (mm)	5
Magnetic type	NdFeB (Neodymium) N50
Resonance (mT)	1400-1450
Coercive force (kA/m)	≤796
Maximum produced energy (kJ/m^3)	382-406
Maximum temperature (°C)	80

2.2 Nanofluid preparation

A base fluid containing TiO_2 nanoparticles (Purity>99.9%) is combined with an agent to obtain a pH of 8 using an ultrasonic device. Because of their high sensitivity to electromagnetic fields, this study's TiO_2 nanoparticles with thermophysical properties were chosen. All nanofluids are ultrasonically excited for three hours with concentrations of 0.015% - 0.075 % by volume, surfactant-free, before pool boiling studies. For stability, the sonicated unit stimulated the nanofluid for 10 minutes hourly. The fluid % absorbance spectra are also evaluated using the Spectrophotometer Ultraviolet (UV-1800) on the first and second days. The stability is still evident because the percentage absorbance spectra on the first and second days were equal, with an inaccuracy of 1.03% (reduced sedimentation of nanoparticles).

2.3 Experimental procedure

With the help of the Variac, the heat input was gradually raised until it reached a critical amount. Then, the heater immediately failed owing to the increased resistance. All experiments were carried out under the specified magnetic fields and boiling pressure. By modifying the coolant flow rate valve, the boiling pressure in the test pool can be changed, and the heat flux may be calculated using the voltage and electric current provided to the cylindrical heater. The experimental conditions of the present study are listed in Table 2.

2.4 Data reduction and uncertainty analysis

The supplied heat rate is calculated using Eq. (1).

$$Q_{heater} = IV \tag{1}$$

The characteristics of nanofluids are ascertained by using the suggested correlations as follows in Eq. (2):[46,47]

$$\rho_{nf} = \phi\rho_P + (1-\phi)\rho_w \tag{2}$$

$$\left(\rho C_p\right)_{nf} = \phi\left(\rho C_p\right)_p + (1-\phi)\left(\rho C_p\right)_w \tag{3}$$

The correlation for nanofluid thermal conductivity is derived from using Eq. (4):[48]

$$k_{nf} = \left[\frac{k_p + 2k_w - 2\phi(k_w - k_p)}{k_p + 2k_w + \phi(k_w - k_p)}\right]k_w \tag{4}$$

where k_{nf} is the thermal conductivity of the nanofluids, k_w is the thermal conductivity of the base fluid and k_p is the thermal conductivity of the nanoparticles.

The following may be used to calculate the *Nu* and *h* using Eq. (5):

$$h = \frac{Q}{A(T_{s,ave} - T_{nf,ave})} = \frac{IV}{\pi DL(T_{s,ave} - T_{nf,ave})} \tag{5}$$

The following factors influence the viscosity of nanofluid using Eq. (6):[49]

$$\mu_{nf} = (1 + 2.5\phi)\mu_w \tag{6}$$

where $T_{nf,ave}$ is the average nanofluids temperature ρ_{nf} is the density of the nanofluids, ρ_p is the density of the nanoparticles, $C_{p,nf}$ is the specific heat of nanofluids, ρ_w is the density of the base fluid, ϕ is the volume fraction of the nanoparticles, D is heater rod diameter, and $T_{s,ave}$ is average heater rod temperature.

Calculations are made for the key parameters derived from the data reduction procedure and the uncertainties of the measurement data.[50] In the case of pool boiling heat transfer coefficients, the most essential parameter's uncertainty does not exceed 5%. The uncertainties can be calculated based on the uncertainty of the instruments (Table 3). Finding the greatest uncertainty of the boiling heat transfer coefficient is possible using Eq. (7).

3. ANN approach

3.1 General of ANN

ANN is one of the most well-known supervised learning methods and models in machine learning. It handles complicated situations very well because it uses enough layers with enough data. One typical use of ANN models is unsupervised learning, which involves learning the input-output relations from a training dataset. The three main components of an ANN design are the input, hidden, and

$$\text{Uncertainty of h} = \sqrt{\left(\frac{\partial h}{\partial V}\Delta V\right) + \left(\frac{\partial h}{\partial I}\Delta I\right) + \left(\frac{\partial h}{\partial T_s}\Delta T_s\right) + \left(\frac{\partial h}{\partial T_f}\Delta T_f\right) + \left(\frac{\partial h}{\partial P_v}\Delta P_v\right)} \tag{7}$$

Table 2: Experimental conditions.

Parameters	Ranges
Power input (W/m^2)	10, 20, 30, 40, 50, 60, 70, 80, 90
Magnetic field, Tesla	0.0008, 0.0010, 0.0012
Pressure, kPa	50, 150, 150
Nanofluid concentration (% by volume)	0.015, 0.025, 0.05, 0.075

Table 3: Uncertainty and accuracy of the instruments.

Instruments	Accuracy	Uncertainty
Voltage supplied by power source, voltage	0.1%	±0.5
Current supplied by power source, ampere	0.1%	±0.5
Digital weight scale, gram	0.01%	±0.01
Thermocouple type T, Data logger, ℃	0.1%	±0.1
Pressure transducer	0.02%	±0.02

output layers. For additional information about the ANN models,[23,24] one of the most exciting areas of artificial intelligence right now is ANN. However, building an ANN is challenging since you have to set up the ANN structure and the parameters in a complicated way. Because of their excellent modeling capability, availability of training procedures, simplicity, and flexibility, nonlinear mathematical models of ANNs are becoming more popular.

Input parameters, the connection weights, are received by the neuron from other neurons before producing an output parameter. The evolutionary approach in this study determined the number of hidden nodes and newly chosen essential attributes. A mathematical methodology for tackling problems with nonlinear regression, ridge regression, is used in this method. Now, we have a well-posed statistical problem with the first one. The Levenberg-Marquardt approach often uses backpropagation to determine the performance's Jacobian 'jX', considering bias factors X and weight. Using the core ideas of this approach, the modification of each variable are calculated using Eqs. (8-10):[24]

$$jj = jX * jX \tag{8}$$

$$je = jX * E \tag{9}$$

$$dX = \frac{-(jj + I * mu)}{je} \tag{10}$$

where E is all errors, I is the identity matrix, and mu is the adaptive controlling parameter.

Linear functions engage the output layer, while tangent functions activate the hidden layer. The backpropagation method determines the degree of error when training. The input data must include specified patterns and objectives to train and test neural networks. Two distinct datasets contain the necessary data: one for training and one for validation. Adjusting the weights and biases may make getting the input data closer to the target outcome possible.

3.2 ANN performance analysis

Evaluating the performance of the improved ANN model compared to the anticipated outcomes allows for analyzing the output results. The following are some examples of how to utilize the correlation coefficient (r) and mean square error (MSE) as distinguishing criteria to evaluate the high accuracy and ensure consistency in the training and forecasting operations of the ANN model using Eq. (11):[29]

$$r = \frac{cov(a,p)}{\sqrt{cov(a,a)\cdot cov(p,p)}} \tag{11}$$

where *cov(a, p)* is the covariance between the sets *a* and *p*, (the measured data and predicted outcomes are determined using Eqs. (12-14):[29]

$$cov(a,p) = E\left[(a-\mu_a)(p-\mu_p)\right] \tag{12}$$

$$cov(a,a) = E\left[(a-\mu_a)^2\right] \tag{13}$$

$$cov(p,p) = E\left[(p-\mu_p)^2\right] \tag{14}$$

where E represents the expected value, whereas μ_a and μ_p represent the mean values of a set and p sets, respectively. Furthermore, *cov(a, a)* and *cov(p, p)* represent the auto covariances of *a* and *p* sets, respectively.

The MSE can be determined from Eq. (15):[29]

$$MSE = \frac{1}{N}\sum_{i=1}^{N}(a_i - p_i)^2 \tag{15}$$

where a_i and p_i are the measured data and predicted results for i set, and N is the number of datasets.

4. Results and discussion

4.1 Verification the measured with the results from correlation

The heat transfer properties of nanofluids in the presence and absence of magnetic fields are explored in this study. The current study's validity is checked to ensure the experimental apparatus is reliable. As it turns out, published data from comparable scenarios does not support the asserted conclusions. Compared to the current experimental data, Fig. 2 displays the anticipated results according to the proposed Cooper correlation.[51] In a mixture of ethyl alcohol and

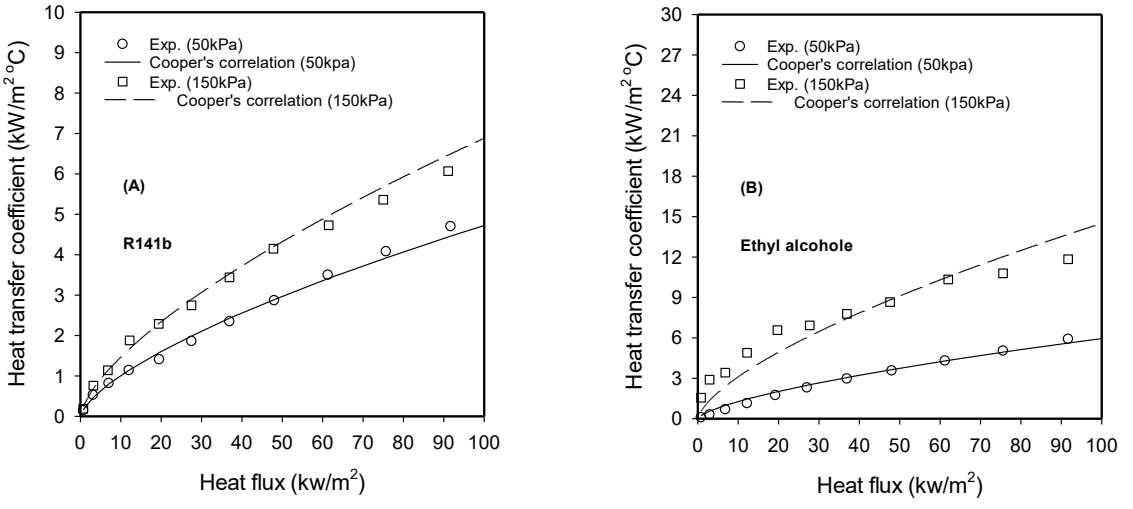

Fig. 2: Comparison of measured heat transfer coefficient with predicted results from correlation with different pressures for (A) R141b (B) ethyl alcohol.[51]

refrigerant R141b, the boiling heat transfer coefficient was measured experimentally, and the results were reasonably in line with the predictions from the Cooper correlation.[51] When comparing experimental results with projected outcomes, the average relative error for ethyl alcohol is 6.62%, and for refrigerant R141b, it is 7.78%.

4.2 ANN structure optimization

Fig. 3 shows the architecture of the ANN model, which consists of four input neurons, two hidden layers with four and twenty neurons, respectively, and a single output neuron. This neural network is a Feed-Forward Neural Network (FNN) that has no backtracking, where data flows directly from the input through the layers to the output. This structure using 2 hidden layers allows the network to learn complex features and improve the accuracy of its predictions. The first hidden layer, often called Hidden Layer 1, receives the input data and employs the Tansig activation function with four neurons, a hyperbolic tangent sigmoid function. This function generously allows the network to learn complex data patterns, with values ranging from -1 to 1. Next, the information is transmitted to Hidden Layer 2, the second hidden layer. This layer likewise has 20 neurons but employs the Logsig activation function, which produces an output value between 0 and 1, making it useful for deep learning and data compression. The tansig function, also known as the hyperbolic tangent function, has several advantages:

- It outputs values between -1 and 1, which helps in centering the data and can lead to faster convergence during training.
- It is a smooth and continuous function, which allows for better gradient flow and reduces the likelihood of vanishing gradients.
- It is helpful for hidden layers in neural networks as it can model complex relationships.

The logsig function, or logistic sigmoid function, also offers distinct benefits:

- It outputs values between 0 and 1, making it suitable for binary classification problems.
- It has a simple derivative, which simplifies the computation during backpropagation.
- It can effectively squash the output, ensuring the model outputs are bounded, which can benefit specific applications.

The R square (Maximum value) will be checked by varying the number from 2 to 20 neurons. After processing from the two hidden layers, the data is sent to the output layer, which has one neuron and uses the Purelin (Linear Activation Function) activation function that does not change the mathematical values much. This makes it suitable for regression forecasting as the input parameters of this model are magnetic field flux (Tesla), nanofluids concentration (%vol.), boiling pressure (kPa), and delta T affect the boiling heat transfer. In contrast, the output parameter is the heat transfer coefficient (kw/m²K) used to evaluate the system's heat transfer. A conventional sensitivity analysis is employed to choose an acceptable model. The neural network structure in this case study is shown in Fig. 3.

The algorithm divides the data into training, validation, and testing sets at random using the Dividerand method as a first step in training the system. This ensures that there is no specific pattern to the data division process. This technique lessens the bias caused by data ordering, which can impact the model's learning, by allowing the model to receive fairly distributed input. Additionally, a Levenberg-Marquardt training method is available (trainlm). Due to its incorporation of both gradient descent and the Gauss-Newton method, this algorithm has gained popularity for neural network training. This makes learning incredibly efficient and quick, which is particularly useful for challenges involving predicting or data sets that are tiny to medium in size. The 468 datasets are

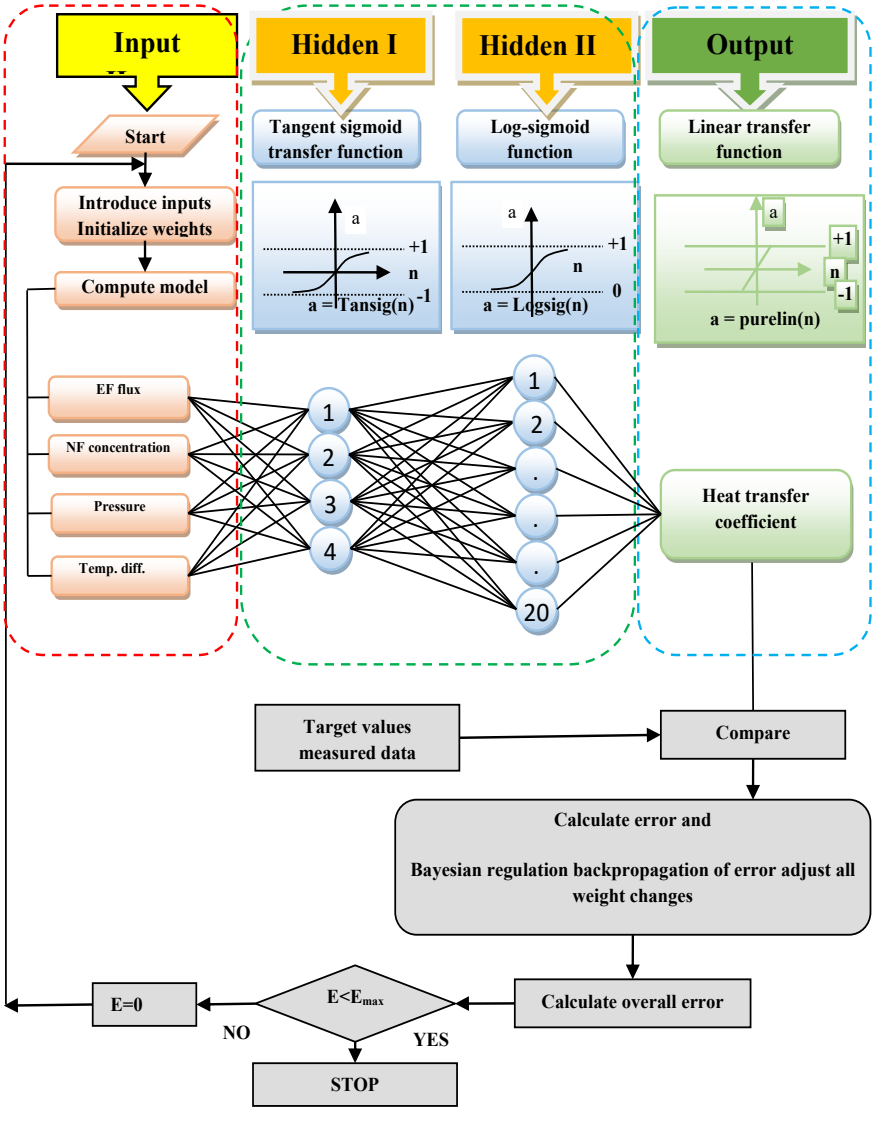

Fig. 3: The proposed optimal ANN model configuration.

separated into 70% training and 15%, 15% for validation and testing categories. The ranges of the datasets are shown in Table 1. Training terminates after the goal MSE is reached or a certain number of epochs have been completed. We selected 328 datasets from the 468 training datasets. The root mean deviation is about 5%, which indicates that the sensitivity was adequate.

A smaller mean squared error (MSE) value indicates a more accurate model, and it is utilized in the performance function section to determine the error between the anticipated results and the observed data. Additionally, MATLAB Executable (MEX) files are specified in calculations. These files contain scripts that compile to C/C++ and enhance computation speed during model training. This technique improves computation efficiency while decreasing the network's training time. Neural networks trained with this architecture perform well in predicting and classifying tasks that demand precise parameters and little tuning time. Based on the data shown in Fig. 4, the number of neurons in the first hidden layer will be 4, and in the second hidden layer will be 20, respectively, leading to the highest R square value.

It is possible to monitor the development of the model's training by looking at the system's training results. Some main metrics are epochs, performance, gradient, mu, and validation tests. The number of iterations the model has learned from the data is referred to by the epoch value. To handle all the data in the training dataset, the model uses one iteration every epoch. Before stopping, the model was trained for 51 iterations in this scenario. The training process ended regardless of the target value being 1000 iterations because the given condition was met, meaning the validation check achieved the desired value. A single second passed, suggesting that the model learned rapidly, maybe because of the simplicity of the network architecture.

The model is learning and improving its accuracy; the performance metrics (the model's error value, like the MSE) went from 109 to 0.0151. MATLAB uses validation checks to stop the training process when the validation error does not decrease continuously to prevent overfitting and improve the model's ability to predict new data. This drop in value shows

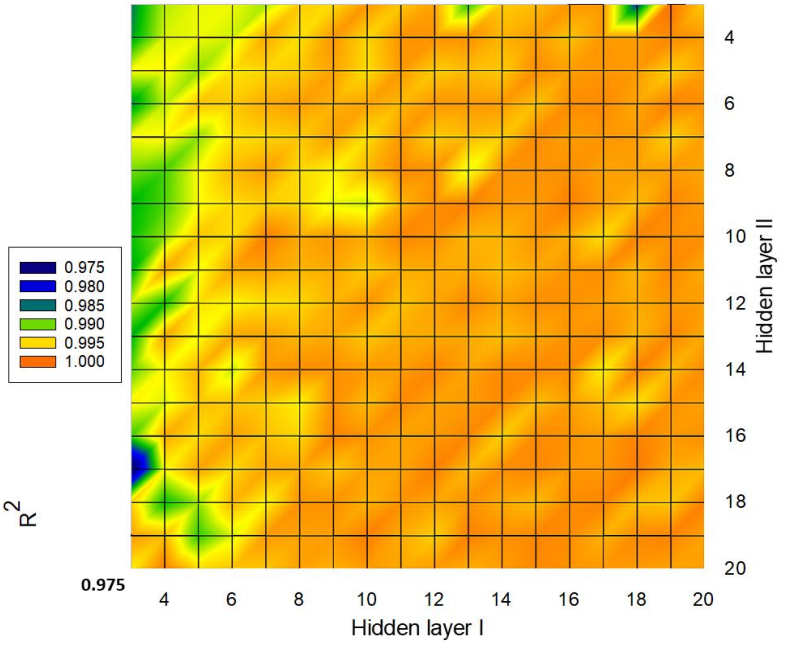

Fig. 4: Variation of R-value with the hidden neuron of hidden layers I and II over testing and overall dataset.

that the model successfully lowers the error. Improving the model's ability to forecast outcomes is indicated by a decrease in the MSE value.

Fig. 5 displays the results of the neural network's training, which assesses the model mainly through the MSE. The curve shown in Fig. 5 consists of three main parts: training (blue), Validation (green), and Testing (red), where the training error continuously decreases, which is the result of the model's parameter updates through the backpropagation and gradient descent processes. The error steadily reduced during the initial 51 training epochs, showing that the model was learning efficiently. At Epoch 45, however, the model achieves its highest performance when tested with data not explicitly utilized for training (MSE = 0.038613), marking the lowest error in the Validation set. If the validation and test errors begin to plateau or rise slightly after Epoch 45, it could indicate overfitting; hence, additional training might not enhance the model's performance.

Fig. 6 depicts the neural network training state, which studies the current neural network model training state. Gradient, mu (Levenberg-Marquardt damping parameter), and validation checks are essential for evaluating the learning process because they determine the model's performance. As illustrated in Fig. 6A, the gradient value is relatively high at

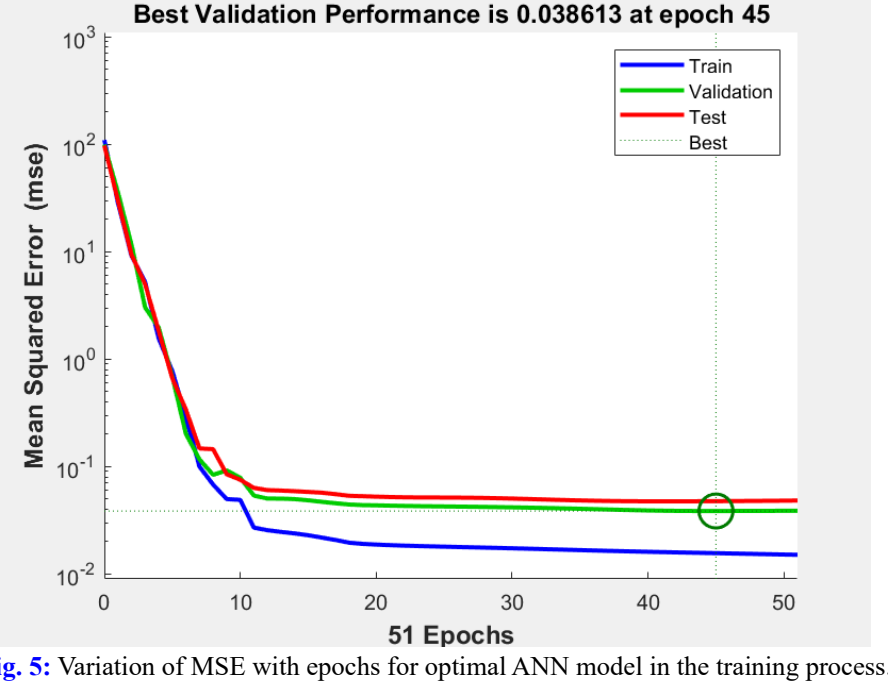

Fig. 5: Variation of MSE with epochs for optimal ANN model in the training process.

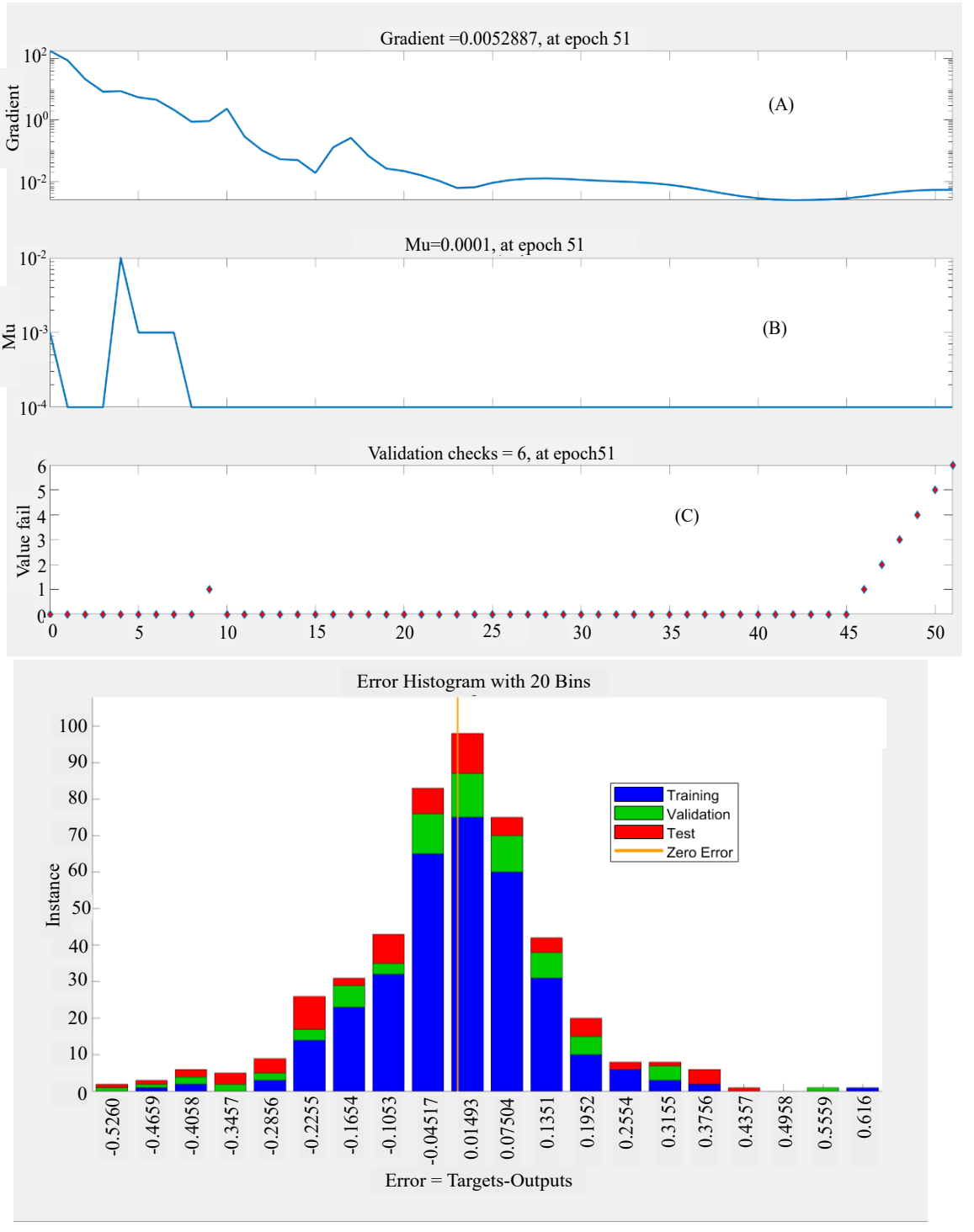

Fig. 6: Variation of (A-C) gradient curve MSE and (D) error histogram in the training process.

the start of training. However, it gradually falls until Epoch 51, when the gradient value drops to 0.0052887, indicating that the model is reaching its optimal value. A decreased gradient suggests that the model is learning and can minimize the error value. However, a very low rate of gradient drop may indicate that the model is approaching the local minimum, at which time it may be unable to improve its results any longer. Being stuck in the regional minimum may cause the model to cease improving, leaving little room for future performance improvement.

As illustrated in Fig. 6B, the value of mu, an essential parameter in the Levenberg-Marquardt Algorithm, is necessary for balancing gradient descent and the Gauss-Newton method. The value of mu changes significantly in the early training phases, reflecting parameter value adjustments to locate the best learning point. However, as the sequence of epochs unfolds, the value of mu gradually drops until, at Epoch 51, it reaches 0.0001. The drop in mu indicates that the

model is entering a state with fewer parameter changes and is determining the ideal value for steady learning. In general, if the value of mu is too significant, the model may learn slowly or be unable to lower the error value sufficiently; if the value is too low, the model may become stuck in a local minimum and fail to adapt to complex input.

The value of the validation checks determines when the model training stops (Fig. 6C). It is shown that the validation checks begin at zero and gradually increase to six at Epoch 51, which is the point at which training stops. When the model can no longer reduce the error of the validation set any further, training is halted to avoid overfitting. Overfitting is a phenomenon in which a model learns so much training data that it cannot accurately predict fresh data. Stopping training allows the model to strike a healthy balance between learning and predicting previously unseen data. This result suggests that the model can learn and properly predict data.

Fig. 6D depicts the error value range of the Histogram. The X-axis represents the error value, which ranges from around -0.5256 to 0.616. In comparison, the Y-axis shows the number of cases with the error value in each range of the Histogram, separated into 20 bins, allowing for a more exact investigation of the error trend. The model's error value is clustered around zero, indicating great prediction accuracy and no significant bias. The error distributions in the training (blue), validation (green), and testing (red) datasets are uniform and within a comparable range, indicating that the model does not suffer from overfitting and can accurately forecast fresh data. Although the overall error value is mainly in the range of -0.1 to 0.1, indicating that the model has high accuracy, there are some outliers with higher than the typical error values at the left and right ends of the graph. This could be due to the nature of the data with high variance or the model's limitation in learning the complex relationships of some data sets. However, the Histogram's error distribution features are similar to the Gaussian distribution, showing that the model is free of systematic bias and may be utilized confidently. If greater performance is sought, regularization, data augmentation, or neural network structure tweaking approaches can minimize mistakes in some cases while increasing the model's capacity to predict more complicated data. The error distribution in training, validation, and testing sets is uniform, with few outliers and no significant data skew, indicating the model is not influenced by high noise. This data demonstrates that the constructed ANN has minimal noise and can predict fresh data.

4.3 Verification ANN results

Regression analysis of ANN compares anticipated results to measured data by analyzing each data set: training, validation, testing, and overall using the primary measure of linear relationship (R^2), which reflects the model's capacity to explain the variability of the data. A value close to 1.0 indicates that the model can accurately predict the value near the actual value. As shown in Fig. 7A, the R^2 value of the training data set is 0.9968, showing that the model can learn the data effectively. The data points are clustered along the perfect fit line, which indicates that the prediction is perfect. Furthermore, the ±5% limits encompass nearly all data points, indicating a minimal and evenly distributed model error.

Figs. 7B and C indicate that the R^2 values for validation and testing data sets are 0.9910 and 0.9890, respectively. These values are still quite high, showing that the model can accurately predict non-training data. However, specific data points start to spread away from the ideal fit line but still within the ±5% Boundaries, indicating that the model performs well without serious overfitting. The testing set's R^2 values show the model's ability to predict new data accurately. As a result, this ANN model has a high degree of generalization, allowing it to be utilized confidently on previously unknown data.

Fig. 7D shows that the model accurately predicts heat transfer coefficient values, with an R^2 value of 0.9949. The data is close to the perfect fit line and within a ±5% error range, indicating a robust model with no evident underfitting or overfitting issues. This result suggests that the constructed ANN model can be used efficiently. However, if additional improvement is required, Regularization Techniques such as L2-regularization, dropout, or adjusting the model structure (Hyperparameter tuning), such as changing the number of hidden layers, may be considered to better deal with the increasing complexity of the data.

4.4 Effects of vapor pressure on boiling heat transfer

The boiling heat transfer process is significantly influenced by vapor pressure. As vapor pressure increases, the boiling point of the liquid also rises, which can affect the heat transfer efficiency. In general, higher vapor pressures can lead to enhanced heat transfer rates due to increased bubble formation and growth. This phenomenon is crucial in various industrial applications, such as in heat exchangers and cooling systems, where optimizing boiling heat transfer is essential for efficiency and performance. Moreover, the relationship between vapor pressure and heat transfer can be complex, as it also depends on factors such as surface characteristics, fluid properties, and flow conditions. Understanding these interactions is vital for engineers and scientists working to improve thermal management systems. Both Figs. 8 and 9 show the changes in the heat transfer coefficient as a function of the temperature differential between the fluid and the heater surface. Both pictures show that the boiling curve increases steeply and moves to the left. Based on the boiling regime, the variation of the heat transfer coefficient with temperature difference shows that the curves cover the natural or free convection and the nucleate boiling. The ANN projected values and the measured data correspond well at 50 kPa, 100 kPa, and 150 kPa pressures. In addition, Figs. 8 and 9 are also compare the ANN predicted results and the measured data. It is found that reasonable agreement is obtained. The statistics indicate a substantial link between pressure and heat transfer rate. The patterns of this study's low boiling pressure findings

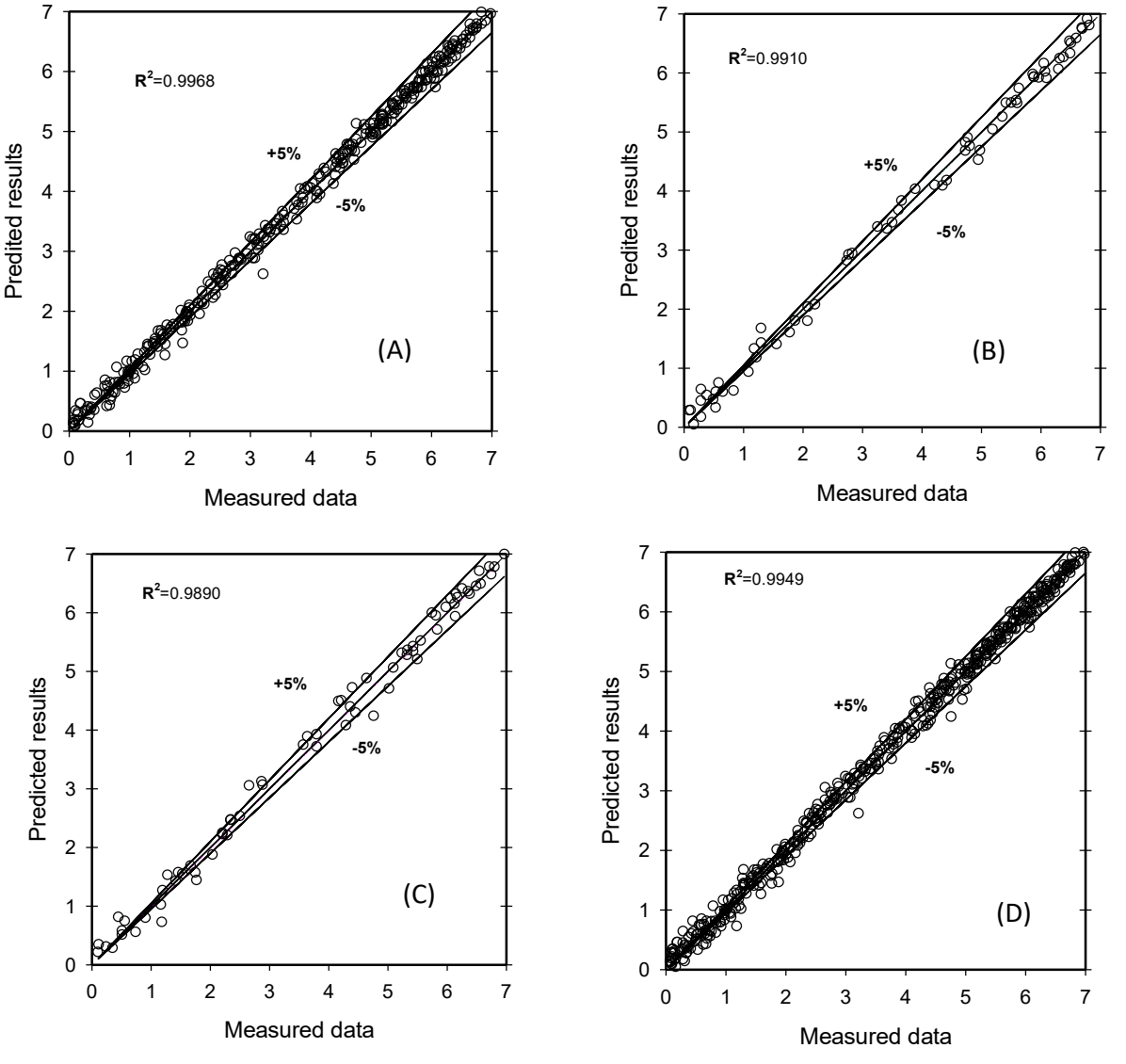

Fig. 7: Comparison of heat transfer coefficient from experiment and ANN for (A) the training dataset, (B) the validation dataset, (C) the testing dataset, and (D) all datasets.

show the changes in the heat transfer coefficient as a function of the temperature differential between the fluid and the heater surface. Both pictures show that the boiling curve increases steeply and moves to the left. Based on the boiling regime, the variation of the heat transfer coefficient with temperature difference shows that the curves cover the natural or free convection and the nucleate boiling. The ANN projected values and the measured data correspond well at 50 kPa, 100 kPa, and 150 kPa pressures. In addition, Figs. 8 and 9 are also compare the ANN predicted results and the measured data. It is found that reasonable agreement is obtained. The statistics indicate a substantial link between pressure and heat transfer rate. The patterns of this study's low boiling pressure findings mirror the boiling behavior for high boiling pressure from Trisaksri *et al*.,[52] as illustrated in Fig. 10.

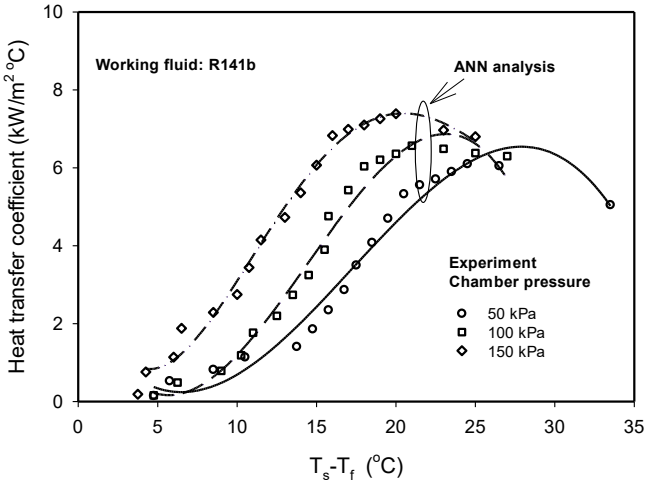

Fig. 8: Variation of heat transfer coefficient with temperature difference for various chamber pressures of R141b.

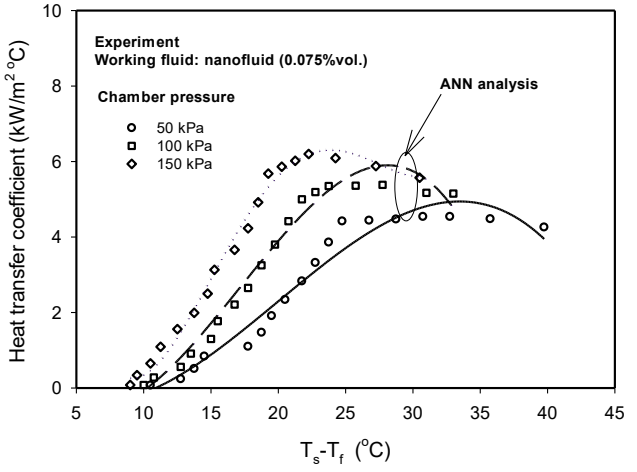

Fig. 9: Variation of heat transfer coefficient with temperature difference for various chamber pressures of nanofluid (0.075%vol.).

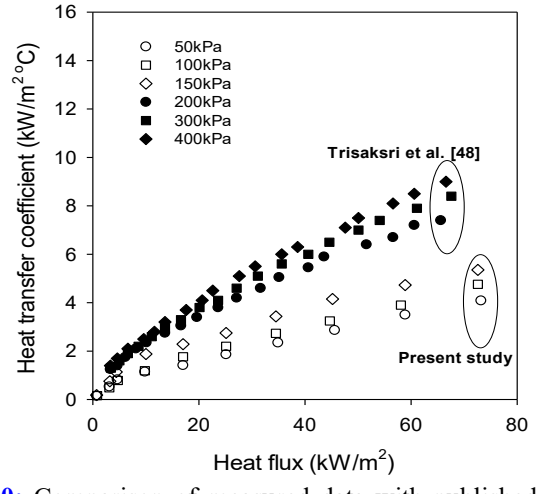

Fig. 10: Comparison of measured data with published data of Trisaksri *et al*.[52]

4.5 Effects of nanofluid concentration on boiling heat transfer

As the liquid begins to boil, tiny, nearly spherical bubbles form on its surface and rapidly rise to the top. Because bubbles deflate quickly, they do not stay on the surface of the boiling liquid for more than a millisecond. With more power applied, the bubbles expand, causing them to vertically merge with smaller bubbles emanating from the same nucleation sites, eventually producing vapor columns. Finally, when this gigantic bubble reaches the critical heat flow, it rapidly collapses into a vapor layer, significantly raising the boiling surface temperature. The film boiling event remained outsids the scope of this experiment. Figs. 11 and 12 depict the boiling phenomena at 50 and 150 kPa boiling pressures, plotted versus nanofluid concentrations. The heat transfer coefficient for pool boiling is highest with pure R141b and considerably decreases with increasing nanofluid concentration. This is because nanoparticles interfere with heat transmission during refrigerant boiling. Nanoparticle deposition on heated surfaces diminishes the density of nucleation sites, reducing boiling heat transfer capacity.[53-55] Some studies believe that adding nanoparticles to a fluid or surface improves heat resistance. Nanoparticle deposition creates a thermal barrier hundreds of times thicker than the exposed heating surface. Experimental results showed that surfaces with a high nanoparticle concentration by volume deposited nanoparticles faster,[56,57] and it is also possible to modify the roughness of the heating surface. In addition, Reasonable agreement is obtained between the ANN predicted results and the measured data.

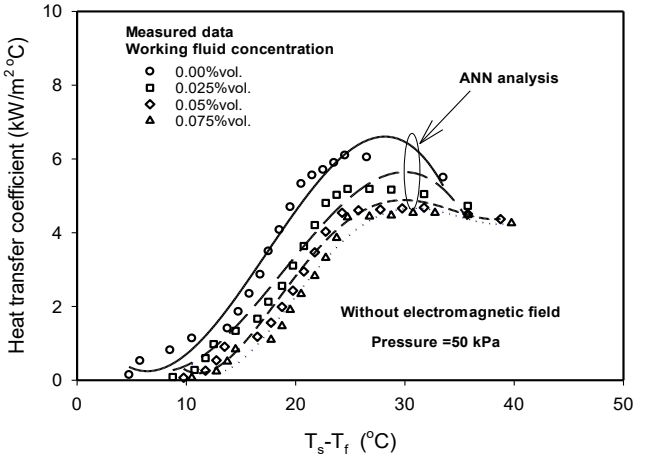

Fig. 11: Variation of heat transfer coefficient with temperature difference for various nanofluid concentrations at a chamber pressure of 50 kPa.

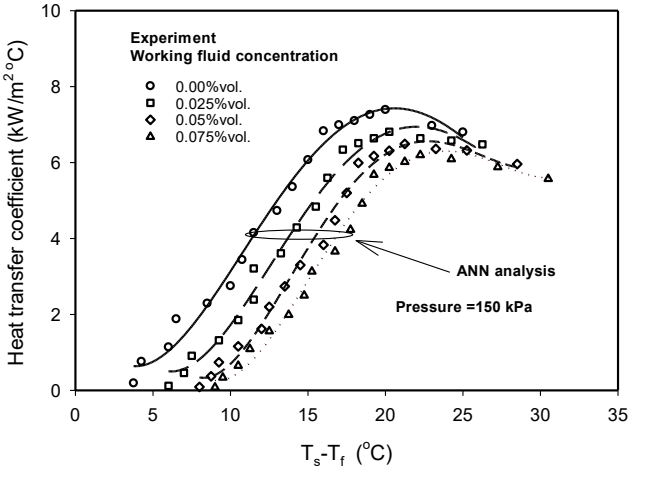

Fig. 12: Variation of heat transfer coefficient with temperature difference for various nanofluid concentrations at a chamber pressure of 150 kPa.

4.6 Effects of magnetic field on boiling heat transfer

Fig. 13 depicts the boiling of refrigerant nanofluids due to a magnetic field. While MF hinders the production of huge vapor columns, the boiling phenomenon is identical to its absence. Nanofluids, which contain nanoparticles, have better thermal properties than regular fluids. A magnetic field can change a nanofluid's flow properties and heat transmission

processes. It has been shown that a magnetic field can increase boiling heat transfer rates by affecting the behavior of nanoparticles in the fluid. The magnetic field can cause nanoparticles to align, potentially improving thermal conductivity and heat transfer efficiency. Furthermore, the interaction between the magnetic field and the nanofluid can cause changes in bubble dynamics during the boiling process. This can impact nucleation sites and bubble growth, affecting total heat transfer performance. Furthermore, the ANN predicted results and observed data show reasonable agreement.

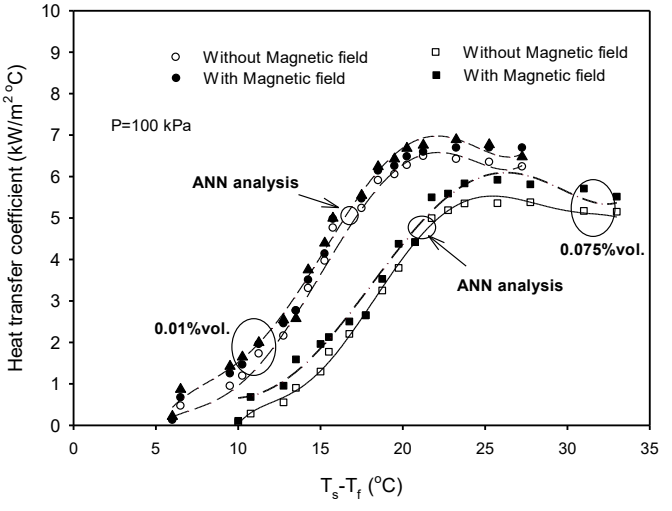

Fig. 13: Variation of heat transfer coefficient with temperature difference with and without magnetic field.

5. Conclusion

To improve heat transfer, the thermophysical characteristics of the working fluid are critical. Thermophysical parameters of nanofluids, including surface tension, latent heat of vaporization, vapor density, and bubble size and frequency, are all susceptible to changes under pressure, which may impact boiling heat transfer. Parameters such as the thermophysical characteristics, boiling surface qualities, and mutual interactions of nanofluids determine how they behave regarding heat transfer during pool boiling. This article develops an ANN model for predicting the boiling heat transfer coefficient in magnetic and non-magnetic environments. The results show that the values measured are relatively close to those the network predicted. With this ANN model, the boiling heat transfer coefficient may be predicted. The MATLAB is a tool that can automatically create and train neural networks. The novelty of this research lies not solely in the use of MATLAB but also in the design approach of neural networks that are appropriate for the problem of predicting the boiling heat transfer coefficient of nanofluids. The boiling pressure, nanofluid concentration, and magnetic field flux significantly affect the boiling heat transfer coefficient. Analyzing the results through regression analysis and error boundaries is ±5% to confirm the efficiency of the ANN through data that are training (70%), validation (15%), and testing (15%). In this research, the error boundaries ±5% were chosen to assess the noise generated in the analysis.

Acknowledgment

The author thanks the Srinakharinwirot University (SWU) Department of Mechanical Engineering for funding this research.

Conflict of Interest

There is no conflict of interest.

Supporting Information

Not applicable.

References

[1] J. H. Lee, T. Lee, Y. H. Jeong, Experimental study on the pool boiling CHF enhancement using magnetite-water nanofluids, *International Journal of Heat and Mass Transfer*, 2012, **55**, 2656-2663, doi: 10.1016/j.ijheatmasstransfer.2011.12.027.

[2] H. Habibi Khoshmehr, A. Saboonchi, M. B. Shafii, N. Jahani, The study of magnetic field implementation on cylinder quenched in boiling Ferro-fluid, *Applied Thermal Engineering*, 2014, **64**, 331-338, doi: 10.1016/j.applthermaleng.2013.11.063.

[3] M. Shojaeian, M. M. Yildizhan, Ö. Coşkun, E. Ozkalay, Y. Tekşen, M. Ali Gulgun, H. F. Y. Acar, A. Koşar, Investigation of change in surface morphology of heated surfaces upon pool boiling of magnetic fluids under magnetic actuation, *Materials Research Express*, 2016, **3**, 096102, doi: 10.1088/2053-1591/3/9/096102.

[4] A. Abdollahi, M. R. Salimpour, N. Etesami, Experimental analysis of magnetic field effect on the pool boiling heat transfer of a ferrofluid, *Applied Thermal Engineering*, 2017, **111**, 1101-1110, doi: 10.1016/j.applthermaleng.2016.10.019.

[5] M. R. Özdemir, A. K. Sadaghiani, A. R. Motezakker, S. S. Parapari, H. S. Park, H. Y. Acar, A. Koşar, Experimental studies on ferrofluid pool boiling in the presence of external magnetic force, *Applied Thermal Engineering*, 2018, **139**, 598-608, doi: 10.1016/j.applthermaleng.2018.05.013.

[6] S. A. Ghauri, M. S. Ansari, Increase of water viscosity under the influence of magnetic field, *Journal of Applied Physics*, 2006, **100**, 066101, doi: 10.1063/1.2347702.

[7] J. Nakagawa, N. Hirota, K. Kitazawa, M. Shoda, Magnetic field enhancement of water vaporization, *Journal of Applied Physics*, 1999, **86**, 2923-2925, doi: 10.1063/1.371144.

[8] X. Pang, B. Deng, Investigation of changes in properties of water under the action of a magnetic field, *Science in China Series G: Physics, Mechanics and Astronomy*, 2008, **51**, 1621-1632, doi: 10.1007/s11433-008-0182-7.

[9] Y. I. Cho, S. H. Lee, Reduction in the surface tension of water due to physical water treatment for fouling control in heat exchangers, *International Communications in Heat and Mass Transfer*, 2005, **32**, 1-9, doi: 10.1016/j.icheatmasstransfer.2004.03.019.

[10] M. Mohammadpourfard, H. Aminfar, M. Sahraro, Numerical simulation of nucleate pool boiling on the horizontal surface for ferrofluid under the effect of non-uniform magnetic field, *Heat and Mass Transfer*, 2014, **50**, 1167-1176, doi: 10.1007/s00231-014-1316-2.
[11] H. Aminfar, M. Mohammadpourfard, M. Sahraro, Numerical simulation of nucleate pool boiling on the horizontal surface for nano-fluid using wall heat flux partitioning method, *Computers & Fluids*, 2012, **66**, 29-38, doi: 10.1016/j.compfluid.2012.05.019.
[12] S. Shuchi, K. Sakatani, H. Yamaguchi, Boiling heat transfer characteristics of binary magnetic fluid flow in a vertical circular pipe with a partly heated region, *Proceedings of the Institution of Mechanical Engineers, Part C: Journal of Mechanical Engineering Science*, 2004, **218**, 223-232, doi: 10.1243/095440604322886964.
[13] S. M. Sami, J. D. Comeau, Influence of magnetic field on two-phase flow convective boiling of some refrigerant mixtures, *International Journal of Energy Research*, 2005, **29**, 1371-1384, doi: 10.1002/er.1122.
[14] T. Lee, J. H. Lee, Y. H. Jeong, Flow boiling critical heat flux characteristics of magnetic nanofluid at atmospheric pressure and low mass flux conditions, *International Journal of Heat and Mass Transfer*, 2013, **56**, 101-106, doi: 10.1016/j.ijheatmasstransfer.2012.09.030.
[15] T. Lee, D. H. Kam, J. H. Lee, Y. H. Jeong, Effects of two-phase flow conditions on flow boiling CHF enhancement of magnetite-water nanofluids, *International Journal of Heat and Mass Transfer*, 2014, **74**, 278-284, doi: 10.1016/j.ijheatmasstransfer.2014.03.028.
[16] H. Aminfar, M. Mohammadpourfard, R. Maroofiazar, Experimental study on the effect of magnetic field on critical heat flux of ferrofluid flow boiling in a vertical annulus, *Experimental Thermal and Fluid Science*, 2014, **58**, 156-169, doi: 10.1016/j.expthermflusci.2014.06.023.
[17] R. Amirzehni, H. Aminfar, M. Mohammadpourfard, Experimental study of magnetic field effect on bubble lift-off diameter in sub-cooled flow boiling, *Experimental Thermal and Fluid Science*, 2017, **89**, 62-71, doi: 10.1016/j.expthermflusci.2017.07.022.
[18] H. Aminfar, M. Mohammadpourfard, R. Maroofiazar, Numerical study of non-uniform magnetic fields effects on subcooled nanofluid flow boiling, *Progress in Nuclear Energy*, 2014, **74**, 232-241, doi: 10.1016/j.pnucene.2014.03.012.
[19] M. Mirzaee, P. Hooshmand, H. Ahmadi, H. Balotaki, H. KhakRah, M. Abdollahzadeh Jamalabadi, Electromagnetohydrodynamic effects on steam bubble formation in vertical heated upward flow, *Energies*, 2016, **9**, 657, doi: 10.3390/en9080657.
[20] M. Mohammadpourfard, H. Aminfar, M. Karimi, Numerical investigation of subcooled boiling characteristics of magnetic nanofluid under the effect of quadrupole magnetic field, *Journal of Engineering Thermophysics*, 2017, **26**, 427-446, doi: 10.1134/S1810232817030122.
[21] C. P. C. Wong, G. C. Vliet, P. S. Schmidt, Magnetic field effects on bubble growth in boiling liquid metals, *Journal of Heat Transfer*, 1978, **100**, 466-472, doi: 10.1115/1.3450832.
[22] S. Kamiyama, J. Ishimoto, Boiling two-phase flows of magnetic fluid in a non-uniform magnetic field, *Journal of Magnetism and Magnetic Materials*, 1995, **149**, 125-131, doi: 10.1016/0304-8853(95)00354-1.
[23] S. A. Kalogirou, Applications of artificial neural-networks for energy systems, *Applied Energy*, 2000, **67**, 17-35, doi: 10.1016/S0306-2619(00)00005-2.
[24] G. J. Zdaniuk, L. M. Chamra, D. Keith Walters, Correlating heat transfer and friction in helically-finned tubes using artificial neural networks, *International Journal of Heat and Mass Transfer*, 2007, **50**, 4713-4723, doi: 10.1016/j.ijheatmasstransfer.2007.03.043.
[25] M. Kahani, G. Vatankhah, Thermal performance prediction of wickless heat pipe with Al_2O_3/water nanofluid using artificial neural network, *Chemical Engineering Communications*, 2019, **206**, 509-523, doi: 10.1080/00986445.2018.1505614.
[26] K. S. Yigit, H. M. Ertunc, Prediction of the air temperature and humidity at the outlet of a cooling coil using neural networks, *International Communications in Heat and Mass Transfer*, 2006, **33**, 898-907, doi: 10.1016/j.icheatmasstransfer.2006.04.003.
[27] G. Xie, B. Sunden, Q. Wang, L. Tang, Performance predictions of laminar and turbulent heat transfer and fluid flow of heat exchangers having large tube-diameter and large tube-row by artificial neural networks, *International Journal of Heat and Mass Transfer*, 2009, **52**, 2484-2497, doi: 10.1016/j.ijheatmasstransfer.2008.10.036.
[28] M. Gao, F. Sun, S. Zhou, Y. Shi, Y. Zhao, N. Wang, Performance prediction of wet cooling tower using artificial neural network under cross-wind conditions, *International Journal of Thermal Sciences*, 2009, **48**, 583-589, doi: 10.1016/j.ijthermalsci.2008.03.012.
[29] N. Bar, T. K. Bandyopadhyay, M. N. Biswas, S. K. Das, Prediction of pressure drop using artificial neural network for non-Newtonian liquid flow through piping components, *Journal of Petroleum Science and Engineering*, 2010, **71**, 187-194, doi: 10.1016/j.petrol.2010.02.001.
[30] M. Hemmat Esfe, H. Rostamian, M. Afrand, A. Karimipour, M. Hassani, Modeling and estimation of thermal conductivity of MgO–water/EG (60: 40) by artificial neural network and correlation, *International Communications in Heat and Mass Transfer*, 2015, **68**, 98-103, doi: 10.1016/j.icheatmasstransfer.2015.08.015.
[31] A. M. Ghahdarijani, F. Hormozi, A. H. Asl, Convective heat transfer and pressure drop study on nanofluids in double-walled reactor by developing an optimal multilayer perceptron artificial neural network, *International Communications in Heat and Mass Transfer*, 2017, **84**, 11-19, doi: 10.1016/j.icheatmasstransfer.2017.03.014.
[32] P. Naphon, S. Wiriyasart, T. Arisariyawong, Artificial neural network analysis the pulsating Nusselt number and friction factor of TiO_2/water nanofluids in the spirally coiled tube with magnetic field, *International Journal of Heat and Mass Transfer*, 2018, **118**, 1152-1159, doi: 10.1016/j.ijheatmasstransfer.2017.11.091.
[33] S. Wiriyasart, P. Suksusron, C. Hommalee, A.

Siricharoenpanich, P. Naphon, Heat transfer enhancement of thermoelectric cooling module with nanofluid and ferrofluid as base fluids, *Case Studies in Thermal Engineering*, 2021, **24**, 100877, doi: 10.1016/j.csite.2021.100877.

[34] P. Naphon, K. Kornkumjayrit, Numerical analysis on the fluid flow and heat transfer in the channel with V-shaped wavy lower plate, *International Communications in Heat and Mass Transfer*, 2008, **35**, 839-843, doi: 10.1016/j.icheatmasstransfer.2008.03.010.

[35] A. Siricharoenpanich, S. Wiriyasart, A. Srichat, P. Naphon, Thermal cooling system with Ag/Fe_3O_4 nanofluids mixture as coolant for electronic devices cooling, *Case Studies in Thermal Engineering*, 2020, **20**, 100641, doi: 10.1016/j.csite.2020.100641.

[36] G. A. Longo, C. Zilio, E. Ceseracciu, M. Reggiani, Application of Artificial Neural Network (ANN) for the prediction of thermal conductivity of oxide–water nanofluids, *Nano Energy*, 2012, **1**, 290-296, doi: 10.1016/j.nanoen.2011.11.007.

[37] M. H. Ahmadi, M. Ghazvini, H. Maddah, M. Kahani, S. Pourfarhang, A. Pourfarhang, S. Z. Heris, Prediction of the pressure drop for CuO/(Ethylene glycol-water) nanofluid flows in the car radiator by means of Artificial Neural Networks analysis integrated with genetic algorithm, *Physica A: Statistical Mechanics and Its Applications*, 2020, **546**, 124008, doi: 10.1016/j.physa.2019.124008.

[38] M. Sadeghzadeh, M. H. Ahmadi, M. Kahani, H. Sakhaeinia, H. Chaji, L. Chen, Smart modeling by using artificial intelligent techniques on thermal performance of flat-plate solar collector using nanofluid, *Energy Science & Engineering*, 2019, **7**, 1649-1658, doi: 10.1002/ese3.381.

[39] S. Panda, A. P. Baag, P. K. Pattnaik, R. Baithalu, S. R. Mishra, Artificial neural network approach to simulate the impact of concentration in optimizing heat transfer rate on water-based hybrid nanofluid under slip conditions: a regression analysis, *Numerical Heat Transfer, Part B: Fundamentals*, 2025, **86**, 2301-2323, doi: 10.1080/10407790.2024.2333944.

[40] A. Ali, M. N. Aslam, M. S. Junaid, M. A. Khan, A. A. Almehizia, Thermal analysis in Darcy-Forchheimer hybrid nanofluid through a Riga plate: an ANN optimization, *Case Studies in Thermal Engineering*, 2024, **60**, 104696, doi: 10.1016/j.csite.2024.104696.

[41] A. M. Alklaibi, K. V. V. C. Mouli, L. S. Sundar, Heat transfer, and friction factor of Fe_3O_4–SiO_2/Water hybrid nanofluids in a plate heat exchanger: Experimental and ANN predictions, *International Journal of Thermal Sciences*, 2024, **195**, 108608, doi: 10.1016/j.ijthermalsci.2023.108608.

[42] M. Yaseen, S. K. Rawat, H. Tyagi, M. Pant, A. Mishra, A. Shafiq, C. S. Ujarari, Artificial neural network with levenberg-marquardt training algorithm for heat transfer analysis of Ag-TiO_2/water hybrid nanofluid flow between two parallel rotating disks, *International Journal of Mathematical, Engineering and Management Sciences*, 2024, **9**, 714-736, doi: 10.33889/ijmems.2024.9.4.037.

[43] Ismail, B. S. Bhadauria, M. Yaseen, S. K. Rawat, M. Pant, Designing machine learning based intelligent network for assessment of heat transfer performance of ternary hybrid nanofluid flow between a cone and a disk: Case of MLP feed forward neural network, *Computers & Mathematics with Applications*, 2024, **169**, 17-38, doi: 10.1016/j.camwa.2024.06.003.

[44] P. Naphon, C. Thongjing, Pool boiling heat transfer characteristics of refrigerant-nanoparticle mixtures, *International Communications in Heat and Mass Transfer*, 2014, **52**, 84-89, doi: 10.1016/j.icheatmasstransfer.2014.01.014.

[45] P. Naphon, Effect of magnetic fields on the boiling heat transfer characteristics of nanofluids, *International Journal of Thermophysics*, 2015, **36**, 2810-2819, doi: 10.1007/s10765-015-1993-1.

[46] B. C. Pak, Y. I. Cho, Hydrodynamic and heat transfer study of dispersed fluids with submicron metallic oxide particles, *Experimental Heat Transfer*, 1998, **11**, 151-170, doi: 10.1080/08916159808946559.

[47] Y. Xuan, W. Roetzel, Conceptions for heat transfer correlation of nanofluids, *International Journal of Heat and Mass Transfer*, 2000, **43**, 3701-3707, doi: 10.1016/S0017-9310(99)00369-5.

[48] J. C. Maxwell, A Treatise on electricity and magnetism, Clarendon Press, Oxford University, UK, 2nd Ed.,1881.

[49] D. A. Drew, Theory of multicomponent fluids, Springer, 1999.

[50] H. W. Coleman, W. G. Steele, Experimental and Uncertainty Analysis for Engineers, John Wiley&Sons, New York, 1989.

[51] M. G. Cooper, Saturation nucleate pool boiling - a simple correlation, *First U.K. National Conference on Heat Transfer*, Amsterdam: Elsevier, 1984, 785-793, doi: 10.1016/b978-0-85295-175-0.50013-8.

[52] V. Trisaksri, S. Wongwises, Nucleate pool boiling heat transfer of TiO_2–R141b nanofluids, *International Journal of Heat and Mass Transfer*, 2009, **52**, 1582-1588, doi: 10.1016/j.ijheatmasstransfer.2008.07.041.

[53] L. Syam Sundar, M. T. Naik, K. V. Sharma, M. K. Singh, T. C. Siva Reddy, Experimental investigation of forced convection heat transfer and friction factor in a tube with Fe_3O_4 magnetic nanofluid, *Experimental Thermal and Fluid Science*, 2012, **37**, 65-71, doi: 10.1016/j.expthermflusci.2011.10.004.

[54] Q. Li, Y. Xuan, Experimental investigation on heat transfer characteristics of magnetic fluid flow around a fine wire under the influence of an external magnetic field, *Experimental Thermal and Fluid Science*, 2009, **33**, 591-596, doi: 10.1016/j.expthermflusci.2008.12.003.

[55] S. Zeinali Heris, M. Nasr Esfahany, S. G. Etemad, Experimental investigation of convective heat transfer of Al_2O_3/water nanofluid in circular tube, *International Journal of Heat and Fluid Flow*, 2007, **28**, 203-210, doi: 10.1016/j.ijheatfluidflow.2006.05.001.

[56] A. K. Tiwari, P. Ghosh, J. Sarkar, Performance comparison of the plate heat exchanger using different nanofluids, *Experimental Thermal and Fluid Science*, 2013, **49**, 141-151, doi:

10.1016/j.expthermflusci.2013.04.012.
[57] F. S. Javadi, S. Sadeghipour, R. Saidur, G. BoroumandJazi, B. Rahmati, M. M. Elias, M. R. Sohel, The effects of nanofluid on thermophysical properties and heat transfer characteristics of a plate heat exchanger, *International Communications in Heat and Mass Transfer*, 2013, **44**, 58-63, doi: 10.1016/j.icheatmasstransfer.2013.03.017.